



# Solar Low Energy X-ray Spectrometer (SoLEXS) on Board Aditya-L1 Mission

K. Sankarasubramanian<sup>1,2</sup> · Monoj Bug<sup>1</sup> · Abhilash Sarwade<sup>1</sup> · Vaishali Sharan<sup>1</sup> · Kumar<sup>1</sup> · Ankur Kushwaha<sup>1</sup> · Smrati Verma<sup>1</sup> · M.C. Ramadevi<sup>1</sup> · Kiran Lakshmi Pathaiah<sup>1</sup> · Mukund Kumar Thakur<sup>1</sup> · Kinshuk Gupta<sup>1</sup> · Nidhi Sharma<sup>1</sup> · Evangelin Leeja Justin<sup>1</sup> · S. Narendra<sup>1</sup> · Abhijit Adoni<sup>1</sup> · Motamarri Srikanth<sup>1</sup> · Vivek Subramanian<sup>1</sup> · Shree Niwas Sahu<sup>1</sup> · Vishnu Kishore Pai<sup>1</sup> · Sajjade Faisal Mustafa<sup>1</sup> · Nashiket Parate<sup>1</sup> · Shamrao<sup>1</sup> · Arjun Dey<sup>1</sup> · Srikanth T<sup>1</sup> · Priyanka Upadhyay<sup>1</sup> · Rethika T<sup>1</sup> · Gayathri Malhotra<sup>1</sup> · S.V. Satyanarayana<sup>1</sup> · Medasani Thejasree<sup>1</sup> · Murugiah S<sup>1</sup> · Naraya Rao G S<sup>1</sup> · Bijaya Kumar Patra<sup>1</sup> · Shalini Maiya<sup>1</sup> · Lakshmi A<sup>1</sup> · Ravi A<sup>1</sup> · Kumar Shivam<sup>1</sup> · Amit Purohit<sup>3</sup>

Received: 30 November 2024 / Accepted: 22 May 2025 / Published online: 25 June 2025

© The Author(s), under exclusive licence to Springer Nature B.V. 2025

## Abstract

The Solar Low-Energy X-ray Spectrometer (SoLEXS) is a moderate spectral resolution ( $\approx 170$  eV at 5.9 keV) instrument with a soft X-ray energy coverage. SoLEXS is one of the experiments on board the Aditya-L1 mission to study the solar atmospheric dynamics along with other remote sensing and in situ payloads. Aditya-L1 was launched in September 2023 and acquired its final orbit at the Sun-Earth Lagrangian point L1 on January 06, 2024. SoLEXS experiment was powered on during December 2023 and is being operated continuously. SoLEXS has observed more than fifty X-class flares and several hundreds of M-class flares so far. This paper provides the details of the SoLEXS instrument along with its capabilities and potential science. This paper also briefly covers the science SoLEXS can provide in combination with other instruments on board Aditya-L1 making it a versatile instrument to study the solar flares and associated phenomena.

**Keywords** Solar flares · Coronal heating · CMEs · Coronal abundances · Silicon drift detectors

## 1. Introduction

Aditya-L1 is envisaged as a mission to study the dynamical nature of the solar corona, the outer layers of the solar atmosphere. Initial studies of these tenuous outer layers were performed only during total solar eclipses in which the high temperature of the corona was

---

✉ K. Sankarasubramanian  
sankark@ursc.gov.in

<sup>1</sup> U R Rao Satellite Centre, ISRO, Bengaluru, Karnataka, India

<sup>2</sup> Centre for Excellence in Space Science and Instrumentation, IISER-Kolkata, Kolkata, India

<sup>3</sup> Indian Space Science Data Centre, ISRO, Bengaluru, Karnataka, India

first discovered Edlén (1943) from the observations of the green emission line of the visible band. Apart from the high temperature of the corona, dynamical phenomena like coronal mass ejections (CMEs) and flares are often present in the corona. Aditya-L1 will also provide data for studying CMEs and its initiation mechanism (Temmer 2021) using the Visible Emission Line Coronagraph (VELC; Raghavendra Prasad et al. 2017). Numerous studies on the properties of CMEs and their relation to flares were undertaken but conclusive understanding behind their relation is yet to be understood (Schmieder, Aulanier, and Vršnak 2015).

The Solar Low-Energy X-ray Spectrometer (SoLEXS) is developed for observing solar flares to obtain (i) data for the study of the DC heating mechanism, (ii) the physical characteristics of the solar flare plasma along with its association to CMEs, (iii) accurate measurements of the coronal temperature (and differential emission measure - DEM) as well as abundances of the coronal plasma. SoLEXS is also configured to provide the flare trigger during a flare to the Solar Ultra-violet Imaging Payload (SUIT, Tripathi et al. 2017) on board Aditya-L1 for high cadence flare observation from SUIT.

The presence of the relatively hot corona (about a million K) compared to chromosphere (about 10,000 to 20,000 K) and photosphere (about 6000 K) is an area yet to be understood. Two mechanisms are behind the high temperature of the corona: (1) waves can carry energy and dissipate them to heat the corona (AC mechanisms or wave-heating mechanisms), (2) flares (including micro- and nano-flares) which may happen all over the Sun can also provide energy for the heating (DC mechanism or reconnection theory). While the VELC can provide data for the first mechanism, SoLEXS will provide data for the second mechanism.

Apart from the high temperature of the corona, there are dynamic phenomena like flares and CMEs which release very high energies in a very short span of time compared to the life time of the activity. The energy released either in the form of high energy photons or in the form of particles affects the space weather conditions. These two dynamic phenomena (flares and CMEs) often occur in conjunction and hence a detailed study of their relationship is important in understanding the energy release mechanism. Recent studies on the association between flares and CMEs (Reva et al. 2024) show a good correlation, meaning most of the CMEs have associated flares. Hence, SoLEXS along with the VELC on board Aditya-L1, which can provide data for CMEs close to the solar disk, can provide the required data to study the flare-CME relation for all class of flares.

In summary, SoLEXS will observe the solar coronal atmosphere (especially high temperature plasma and its dynamics) and provide (i) data for the study of the DC heating mechanism complementary to the data from the VELC, (ii) the physical characteristics of solar flares ranging from the X-class to the CME association along with coronagraph data, and (iii) independently measure the coronal temperature (and differential emission measure - DEM) as well as abundances of the coronal plasma.

## 2. Science Objectives

The primary science objectives of the SoLEXS payload are the following:

- To understand solar flares and the coronal heating mechanism
- Quantitatively measure coronal abundances and hence the first ionization potential (FIP) effect
- Association of flares and CMEs using CME data from Aditya-L1 and/or any other observatories
- Flare and prominence eruption studies using prominence data from Aditya-L1 and/or any other observatories operating during this period

## 2.1. Flares and Coronal Heating

Although the solar corona has been observed and studied in detail for a long time, the high temperature of the corona has not yet been fully understood (Sakurai 2017). It is observed that weaker flares occur more often than larger flares (Hudson 1991) and hence weaker flares are possible candidates for the high temperature of solar corona especially during the quiet-Sun period. For sufficient coronal heating, the index in the power-law relation between the flare occurrence and its energy has to be about  $-2.0$  (Aschwanden 2004). The derived power-law index varies from  $-1.4$  to  $-2.8$  obtained with different instruments of varying spectral and spatial resolution (Aschwanden 2004). Although the Reuven Ramaty High Energy Solar Spectroscopic Imager (RHESSI) has allowed the study of thermal and non-thermal energy contents in microflares systematically, the uncertainty remains in separating the thermal from the nonthermal energy due to instrumental effects and biases.

Hannah et al. (2008, 2011) and Christe et al. (2008) discussed the implications of fitting a power law to the RHESSI data due to two reasons: (i) turnover at lower energies and (ii) steeper cut-off at higher energies. Figure 2.1 in Hannah et al. (2011) shows a typical frequency distribution of flare thermal energy from different observations. RHESSI data, which are the only high spectral resolution data in this figure (and were available during that time), clearly show the two effects above. The reason for (i) is missing for smaller events due to insufficient counts to find and successfully analyse them, whereas for (ii) it is due to the attenuating shutter that increases the low-energy cut-off. It should also be noted that these turnovers can also occur due to a basic physical mechanism even if the instrument is infinitely sensitive (Sakurai 2017; also refer to Figure 10 in Sakurai 2017).

Although, RHESSI has allowed the study of thermal and nonthermal energy contents in microflares systematically (Hannah et al. 2008), the uncertainty remains in separating the thermal from nonthermal due to instrumental effects and biases. In order to overcome these limitations, an instrument with better energy resolution and lower background is necessary to unambiguously study the energy contents of microflares. Such instruments are already flown (XSM on Chandrayaan-1 and - 2 around Moon - Vadawale et al. 2014; Alha et al. 2008; Huovelin et al. 2002; the Miniature X-ray Solar Spectrometer (MinXSS) series from low-Earth orbit - Moore et al. 2018). Recently, Valluvan et al. (2024) have studied all flares from XSM on board Chandrayaan-2 and derived the power law to be close to 2 (1.96), indicating that nanoflares do play a significant role in coronal heating (Figure 10 in Valluvan et al. 2024). Upendran et al. (2022) studied nanoflare heating in the solar corona using X-ray observations from XSM (Solar X-ray Monitor) on board Chandrayaan-2. They derived typical impulsive event frequencies, timescales, amplitudes, and the distribution of amplitudes for nanoflares. A very recent study by Aschwanden (2025) showed that the majority of astrophysical cases follow the fractal-diffusive self-organized criticality (FD-SOC) model for the frequency distribution of fluxes and fluences with a power-law distribution of 1.8 for flux and 1.67 for fluences. Aschwanden, Carolus, and Schrijver (2025) found that such SOC model works for stellar flares also covering almost 13-orders of magnitude. SoLEXS will be one such instrument similar to the ones above, but its location advantage can provide 100% duty cycle compared to any X-ray instruments flown before. Also, SoLEXS sensitivity will be an order of magnitude more than XSM on Chandrayaan-2 especially during quiet solar conditions due to its larger aperture size.

## 2.2. Elemental Abundances and FIP

It is well known that the coronal abundances of low FIP elements ( $< 10$  eV) are enhanced compared to the high FIP elements. Such anomaly is also seen in other Sun-like stars having

corona. However, it has been consistently seen by the high spectral resolution instrument that the fractionation of the Fe abundance is always higher within the low FIP elements compared to Si (which has a FIP almost similar to that of Fe). This is a prediction from recent theoretical studies (Laming 2015). Recent studies of elemental abundances using data from the XSM on board Chandrayaan-1 (Narendranath et al. 2020, 2014) and Chandrayaan-2 (Mondal et al. 2023; Nama et al. 2022; Mondal et al. 2021) confirm the higher fractionation of Fe abundances, as observed by the high spectral resolution instrument, which also varies during a solar flare (see Figure 3 in Narendranath et al. 2020). It is now well understood that the low FIP elements are enhanced during the quiet period and they decrease towards a photospheric abundance level during flares, as seen in Figure 3 of Narendranath et al. (2020). This gives us the confidence that the spectral resolution achieved on board by Chandrayaan-1 and 2 is more than sufficient to study the FIP effect and also the variability of the abundances during flares (Narendranath et al. 2020; Mondal et al. 2021). With the recent theoretical developments of using Alfvén waves to understand the FIP effect (Laming 2021), SoLEXS will be an ideal instrument to provide a wealth of data covering the full range of flares to study the elemental abundances and the FIP effects. More recently Lee et al. (2025) studied the effect of waves on the fractionization of elements such as Si X (low FIP) and S X (high FIP). They showed that there is a strong correlation between the chromospheric transverse MHD waves with the coronal abundance fractionization. Aditya-L1 instruments, SoLEXS and the SUIT can study this relation further. For a detailed list of lines and its potential to derive the physical quantities refer Del Zanna and Mason (2018).

RHESSI (Lin et al. 2002; Smith et al. 2002), used by many solar observers around the world, has a spectral resolution of about 1 keV. Though it covers a large energy range, it misses out critical spectral information below 3 keV. Crystal type spectrometers, for example RESIK (REntgenovsky Spektrometres Izognutymi Kristalam; Sylwester et al. 1998), whose spectral resolution are typically two orders better, does not have the capability to cover the large energy range required for generating the spectra and provides no measure of the X-ray continuum emission essential to derive the thermal and nonthermal energies.

Most of the solar X-ray observations with recent missions, like Hinode (Golub et al. 2007), are aimed at to study the locations of the flares and hence carry out high spatial resolution observations without good spectral information.

### 2.3. Flare-CME Association

Even though the proposed SoLEXS instrument may not see CMEs directly, its data will be very valuable for the study of flare related CMEs. Yashiro and Gopalswamy (2009) studied the correlation between different physical quantities relating the X-ray flare observations with the optical observations of CMEs. They found a high correlation ( $\approx 0.62$ ) between the flare fluence and CME kinetic energy. High correlations will be expected if the physical mechanisms behind flares and CMEs are the same or similar. Their observations suggest that the lower the peak X-ray flux of the flare the weaker is the CME association. Their study also confirmed that long duration events (LDEs) observed in X-rays usually produce CMEs. Recent studies with Fermi flare data clearly bring out that the flare related CMEs are generated during the pre-flare or rising phase of the flares (Mawad, Abdel-Sattar, and Farid 2021). With the CMEs detected closer to the solar disk with VELC and also weaker flares observed with SoLEXS, any observational bias if at all exists, as in Figure 1 of Yashiro and Gopalswamy (2009), can be studied.

Most recent study by da Silva et al. (2023) looked for higher temperature plasma during or before the flare events as an evidence for reconnection and hence CME. They used data

of the Mg XII spectroheliograph on board the Complex Orbital Observations Near-Earth of Activity on the Sun (CORONAS-F) satellite which is sensitive to hotter plasma (temperature above 4 MK). Their results show that for stronger flares, reconnection is the dominant mechanism while other mechanisms may play a role for weaker flares. da Silva et al. (2023) statistically studied the hotter nature of the plasma before solar flares, considered as onset temperature, for solar flares in the 2010 to 2011 period. They concluded that about two-third of flares show hot onset temperature above 8.6 MK with a small variation in the emission measure indicating that a small volume of plasma is heated to high temperatures. Hudson (2025) studied the hot onset precursor event (HOPE) using the emission measure-temperature relation before the flare onset and showed that HOPE appears as a “horizontal branch” before the nonthermal impulsive phase of the solar flare. A flare anticipation index (FAI) was derived using this to anticipate flares before few minutes of the flares. The FAI is derived using the GOES data. With SoLEXS spectroscopic capabilities, HOPE studies and also the FAI can be carried out regularly.

#### 2.4. Flare-Prominence (Filament) Eruption Studies

The relation between the prominence eruption and solar flares has been of interest for the physics of the large scale reconnection mechanism since prominence eruptions are related to large scales while flares can be localized. Prominence (filament) eruptions can be of full or partial or confined characteristics depending on the eruption configuration: full – entire magnetic structure erupts along with the plasma expelled into the heliosphere, partial - entire or partial magnetic structure erupts along with partial or no material expulsion, confined – no filament mass and the supporting magnetic structure escape from the Sun (Gilbert, Alexander, and Liu 2007). Further, based on the radial and transverse motion, the filament/prominence eruption is highly associated with CMEs with radial events (Gopalswamy et al. 2003). Understanding the relation between the solar flares and flare-prominence eruptions will provide the physics behind the large scale eruptive phenomenon on the Sun (Koleva, Dechev, and Duchlev 2021).

Recent studies of filament eruptions driven by reconnection have brought out new findings. Li et al. (2025) showed an observation of failed eruptions which are predicted by numerous studies but rarely observed indicating the importance of surrounding magnetic field structures for coronal mass ejections or failed eruptions. Ng, Zhang, and Chen (2025) studied a peculiar feature in the FIP for a flare on 16 February 2024. They observed that the depletion of low-FIP elements occurred well before this particular flare. This particular flare was associated with a newly developed filament. They concluded from these observations that the reconnection happened in the chromosphere rather than in the corona.

Aditya-L1 carries an imaging payload called the Solar Ultra-violet Imaging Telescope (SUIT) (Tripathi et al. 2017). This imaging payload along with X-ray payloads (Sankara-subramanian et al. 2017) will enable the study of solar flare energetics. Both these payloads observe solar flares at two different wavelengths and at two different heights in the solar atmosphere. The data required for the proposed studies are available from both of these instruments.

### 3. SoLEXS Requirements

The flux of the Sun in the low energy range of 1.5–12.5 keV (or 1–8 Å in GOES range) is very high ( $10^{-8}$  W m $^{-2}$ ) and variable. The solar X-ray spectra are generally soft, with

**Table 1** Science Requirements, critical instrument parameters, and the achieved on board performance of SoLEXS.

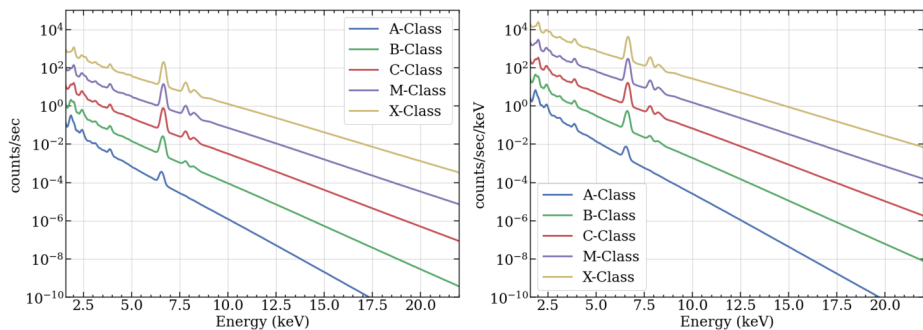
| Science goals                           | Critical inst. requirement  | On board performance  |
|---|---|---|
| Flare studies – Flare heating           | Energy range: 1–15 keV<br>Flare coverage <A-class to X-class                        | Energy range: 2–22 keV<br>> C-class due to solar maximum        |
| Flare studies - Pre-cursor activities   | Spectral res: < 500 eV  | 170 eV at 6 keV   |
| Coronal studies – Coronal abundances    | Spectral res: < 250 eV<br>Energy range: 1–10 keV<br>Timing: better than few seconds | 170 eV at 6 keV<br>Energy range: 2–22 keV<br>One second spectra |
| Coronal studies – Flare-CME association | Timing: better than few seconds<br>Flare coverage: <A-class to X-class              | One second timing<br>> C-class due to solar maximum             |

most of the photons concentrated at energies around and below 3 keV. The variability, during flares, is mostly at higher energies associated with variable high temperature. Photon flux for an A-class flare, at 1 AU and over 1–10 keV, is typically  $10^4$  photons sec $^{-1}$  cm $^{-2}$  whereas for X-class flare it is  $5 \times 10^7$  photons sec $^{-1}$  cm $^{-2}$ . Hence, this range requires a detector with a large dynamic span capability. With the current technology, a single detector cannot provide such a large dynamic range without using attenuators, as done in RHESSI and in XSM on board Chandrayaan-2. SoLEXS is configured with two detectors (SDD1 and SDD2) along with the required apertures of different diameter to cover the full dynamic range of solar flares using either of the detectors. SoLEXS with two detectors behind two apertures would provide a count rate of about  $6 \times 10^5$  counts for the large aperture and 9500 counts for the small aperture for an X1.0 class flare at 1 keV. Due to the high count rate in SDD1, spectra from SDD2 might be used for big flares. For the same flare at 20 keV, the count rate would be 0.3 counts sec $^{-1}$  and 0.005 counts sec $^{-1}$  for SDD1 and SDD2, respectively. The sudden drop in the count rate is due to the steep spectra in the X-ray energy band.

To study the detailed emission mechanisms and abundances during flares, a moderate spectral resolution is a must. Most of the spectral lines present in the solar corona are at the soft X-ray regime, below 10 keV. Many emission lines are seen below 3 keV, hence a spectral resolution better than 250 eV at 6 keV (similar to that of XSM on Chandrayaan-1 and Chandrayaan-2) will be required. SoLEXS is aimed at providing a spectral resolution  $\leq 250$  eV at 5.9 keV and observe low energies down to  $\approx 1$  keV in order to observe as many spectral lines as possible.

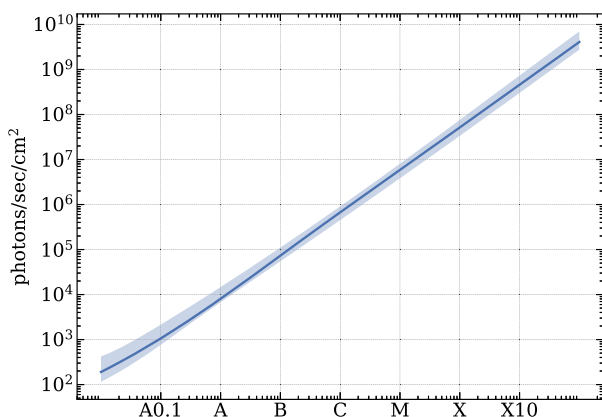
The solar corona contains highly charged H- and He-like ions of many elements. While the Chianti atomic database provides all the potential line lists (Dere et al. 1997), major elements, which show emission features in the energy range of 1–10 keV, are provided in Table 1 of Sylwester et al. (1998). As can be seen from this table, the abundant elements are Al, Si, S, Ar, Ca, Fe, and Ni. While a crystal based spectrometer (Sylwester et al. 1998) provides high spectral resolution to resolve many satellite lines, the energy range is limited. The silicon detector based spectrometers provide larger energy coverage but lack the spectral resolution to resolve the satellite lines in the iron complex. However, a moderate spectral resolution of better than 250 eV at 6 keV will be able to separate the ions as well as bring out the emission features above the local continuum emission as seen by earlier silicon based spectrometers (Vadawale et al. 2014; Alha et al. 2008).

Table 1 provides the basic requirement for the SoLEXS instrument to meet the science objectives as stated above. The last column of this table provides the relevant performance



**Figure 1** Left: Expected energy spectra from SoLEXS with respect to different GOES class solar flares for the small aperture of SoLEXS. The spectra include the spectral redistribution function (Section 5.1.3) as well as the collimator response (Section 5.1.5) of SoLEXS. Right: Same spectra in count rate units per keV.

**Figure 2** Count rate estimated for different GOES class flares over the energy range of 1–10 keV. The shaded regions are the photon statistics to indicate the typical variability.



achieved on board after optimizing the operating conditions. For the flare studies and flare heating, especially in calculating the energy, additional data from SUIT or any other imaging instruments would be required to estimate the flare volume and hence the thermal energy content of the flares. For the flare-CME studies, CME data either from the coronagraph on board Aditya-L1 or any other coronagraph data would be required.

Figure 1 shows the expected count rate for the small aperture SDD. The ratio of area between the large to the small aperture is 67, meaning that the large aperture spectra can be obtained by multiplying per 67 the small aperture spectra. The count rate unit is used for the flux received at SoLEXS in order for the readers to understand the typical signal levels per bin of SoLEXS. The count rate per keV is also provided for understanding in standard units to compare it with other instruments.

The dynamic range of the detector depends on its count rate capability. Figure 2 shows the integrated count rate for different GOES class flares in the energy range of 1–10 keV. The x-axis shows the GOES classification of solar flares. To cover X-class flares (few times  $10^8 \text{ photons sec}^{-1} \text{ cm}^{-2}$ ), an aperture of  $0.1 \text{ mm}^2$  or smaller is required. This assumes that the system is 100% efficient. In reality, the efficiency of the detector system will be lower due to the Be-window (used to avoid optical light) in front of the detector. At higher energy ( $> 10 \text{ keV}$ ), the limited depth of depletion will reduce the efficiency to lower values. SoLEXS was designed with two apertures of area  $7 \text{ mm}^2$  and  $0.07 \text{ mm}^2$ , respectively to

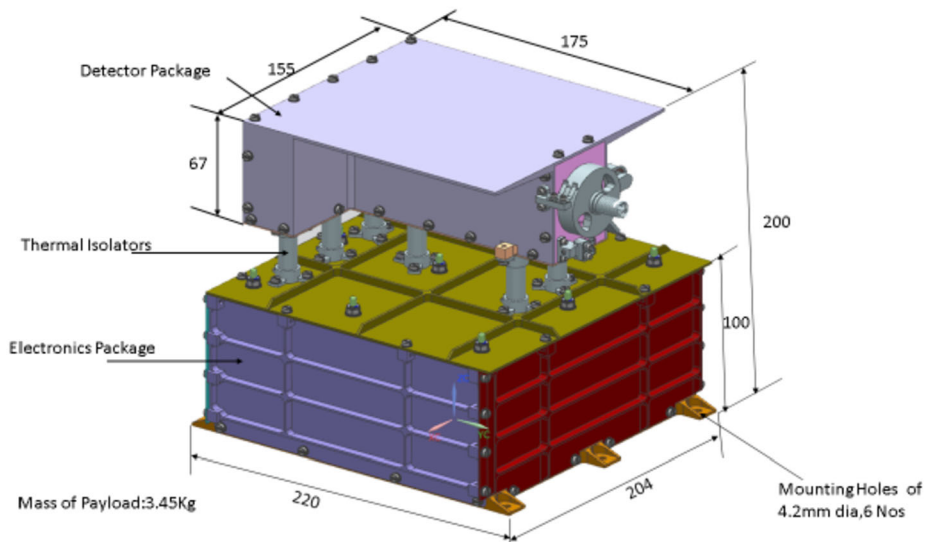


**Figure 3** SoLEXS is configured as a single package with two modules (Detector and Electronics Modules). All dimensions in this figure are in millimeters (mm).

cover the full dynamic range (C-class and above with a small aperture and < C-class with a larger aperture).

## 4. Payload Configuration

SoLEXS is mechanically configured as two modules combined into a single package as shown in Figure 3. Two modules, namely detector and electronics modules, are required in order to keep the thermal control requirements of the detector module to its minimum.

### 4.1. Detector Module

The detector module consists of two milled covers: 1) bottom U cover and 2) top cover. These are machined from a single block of aluminum Al6061-T65. The bottom U-cover and the sectorial view of a detector mounted on the PCB is shown in the top picture of Figure 4. The bottom picture in Figure 4 shows the top cover of the detector module. On one side of the bottom cover, a PCB is mounted using six M3 screws on which two identical detectors are mounted, as shown in the inset of the bottom figure. Detector pins are connected to the PCB through sockets and the sockets are soldered (not shown in this Figure). Two thermal flanges are fastened to the two detector studs through the back plate to transfer the heat generated by the detector (marked in Figure 4).

On the other side of the bottom U cover in the top picture of Figure 4, an on board calibration source holder is mounted (marked as radioactive source). A single Fe55 radioactive source is mounted along with a titanium foil in such a way that the K-alpha and K-beta photons of Mn and the fluorescence of Ti reach the detector for regular calibration purposes. The source is selected such a way that its maximum strength is less than 0.1 photons per sec at the detector plane. This allows SoLEXS detectors to have regular calibration over the

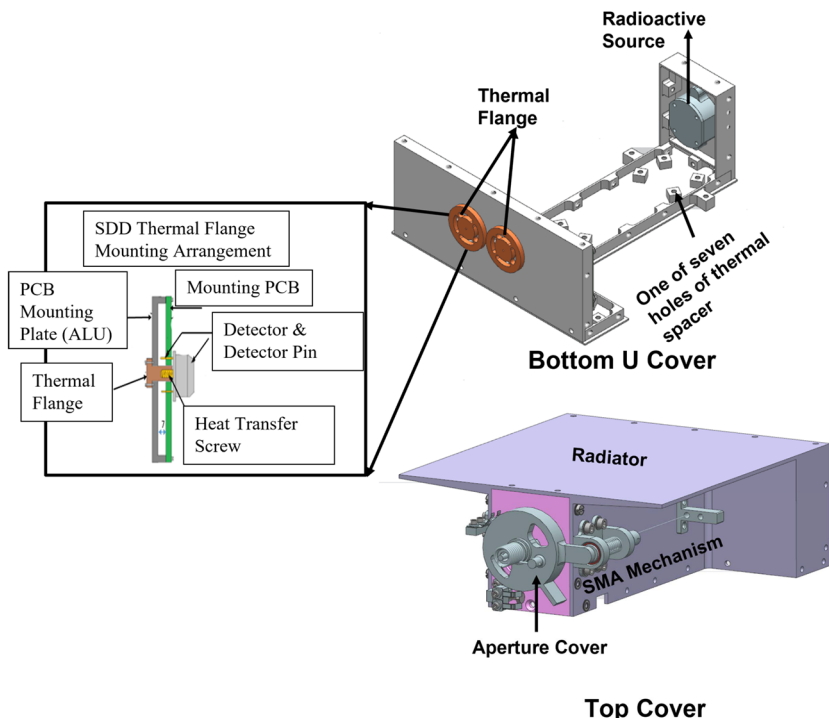


**Figure 4** Top: Bottom U cover for the detector module containing the thermal flange, which is mounted behind the detector and supported by the backplane of the U cover. Front plane has a radioactive source inside a holder. The inset in this figure shows how the detector is mounted to the PCB and mechanically attached to the thermal flange along with the back plate. Bottom: Top cover of the detector module showing the aperture cover mechanism. The top plate of the top cover acts as a radiator. The top and bottom figures are rotated by  $180^\circ$  to show both the front and back planes. When mounted, the aperture cover in the bottom figure will come in the side of the radioactive source of the top cover. The Sun direction is towards the radioactive source plane.

life time of the mission. The count rate is such that the characteristic lines of the radioactive source do not show significant counts for one minute or lesser duration. Longer time integration during the quiet period of the Sun and/or observations of dark sky (planned to be carried out regularly) will be used to study the energy resolution of the detectors.

Adjacent to the calibration radioactive source are two apertures (not seen in Figure 4) through which solar X-ray photons reach the detector. The apertures are cylindrical in nature and have a measured area of  $0.106 \text{ mm}^2$  and  $7.106 \text{ mm}^2$ , respectively. The detector with larger aperture in front is referred as SDD1 and the detector with small aperture as SDD2. This nomenclature will be followed throughout this paper. The aperture hole size, the distance between the detector, and the aperture decides the field of view (FOV) coverage of the detectors. SDD1 has a full width zero maximum FOV of  $\pm 1.8^\circ$  cone and the same for SDD2 is  $\pm 1.3^\circ$ .

The bottom L-shaped detector module (as shown in the top picture of Figure 4) is made as a single unit, in order not to lose the alignment between the aperture hole (in the front plane) and the detectors (in the back plane).

The detector package and the electronics package are mechanically interfaced by seven spacers (made out of glass fiber reinforced polymer (GFRP)), which serves as thermal iso-

lator and mechanical support to the detector package. The seven GFRP stands are also used to anchor the detector module on top of the electronics module. The separation between the two were optimized to keep the resources to the minimum and still maintain the detectors at the required temperature and also keeping the rigidity of the detector package for vibration.

The top cover of the detector module is also machined from a single aluminium block, it has an inverted U section and the top portion is extended to a larger area that will cater as radiator, as marked in the bottom picture of Figure 4. The whole detector module is made out of 3 mm aluminium alloy along with an aperture cover mechanism to protect the detectors and apertures from dust. Also, the cover mechanism will minimize the particle dose experienced by the detectors during the Van-Allen belt passage during the Earth orbit phase of the mission. The thickness of the package is arrived at after carrying out the dosage experienced by the detectors in this mechanical configuration through a SPENVIS simulation for the planned five years of the mission life, including the Earth bound orbit. This protection ensures that the detector leakage current is minimal during the initial phase of operation and the spectral resolution will not degrade more than 250 eV at 6 keV over the anticipated five-year mission.

The top cover is also the anchoring place for the aperture cover mechanism as shown in Figure 4. A Shape Memory Alloy (SMA) based mechanism is used for the aperture cover mechanism of SoLEXS. As shown in Figure 4, the opening position of the cover mechanism is kept at about 45 degree from that in its stowed configuration. At the final L1 orbit, the one-time operation mechanism is enabled by heating the SMA to rotate the aperture cover mechanism to its final position. As this is one time operation, a calibration in closed condition with the source within the detector box is carried out before operating the mechanism.

Two Silicon Drift Detectors (SDD) are used in SoLEXS. SDDs are a new type of detectors, which are Si-based with low anode-capacitance and low leakage current, yielding good spectroscopic performance. They are chosen mainly because of their large dynamic range capability as well as spectral resolution under nominal cooling compared to the conventional Si-PIN used in earlier missions (for example XSM on board Chandrayaan-1). SDDs are tested for performance in laboratories and flown on board NASA's APXS in the Mars Exploration Rover and also in XSM on board Chandrayaan-2 and MinXSS. The efficiency at lower energies can be low due to the entrance window used to cut-off visible light. For a  $12.5\ \mu\text{m}$  thick Be window, the efficiency is about  $\approx 20\%$  at around 1 keV. SoLEXS uses  $8\ \mu\text{m}$  thick Be window to have higher efficiency in the 1 keV range. The efficiency at 30 keV will fall down to  $\approx 30\%$  for a  $450\ \mu\text{m}$  active depth of the detector, which is the case for SoLEXS. Detector cooling is achieved using a two-stage Peltier cooler integrated within the detector. The typical temperature of the detector achieved on board is about  $-45\ ^\circ\text{C}$  for a detector box temperature of  $-15\ ^\circ\text{C}$ . Table 1 lists the achieved instrument parameters of SoLEXS.

The SDD module (active physical area of  $30\ \text{mm}^2$ ) from PN-Sensor, Germany (part SDD-30-130PNW-TOXSL), with TOX-SL package is used in SoLEXS. Few detector pins of the SDD used in SoLEXS are highly ESD sensitive to undergo any direct soldering. As suggested by the manufacturer, detectors were mounted on sockets. As this is a new process, it required space qualification. The mounting process qualification of the detectors on the PCB were carried out before applying the process for the flight model of SoLEXS. Details of the process qualification are outside the scope of this paper.

## 4.2. Electronics Module

The second module in SoLEXS package is the ‘Electronics Module’. The overall end-to-end functional electronics block diagram is shown in Figure 5. As discussed in the earlier

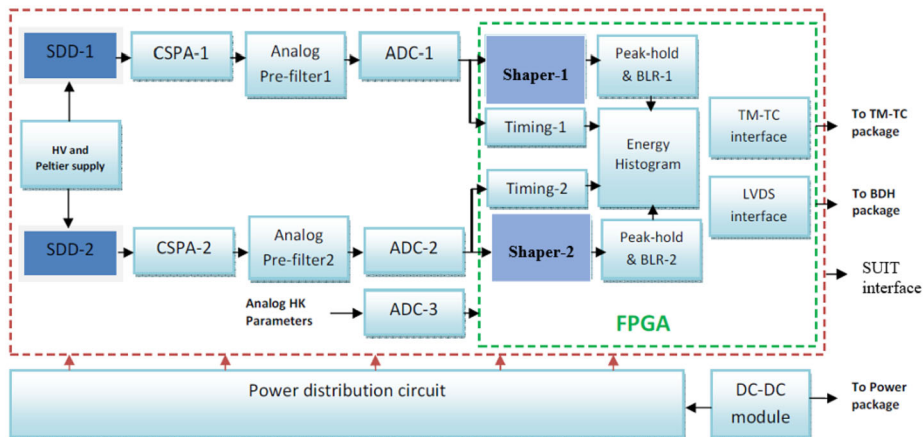


**Figure 5** Electronics configuration of SoLEXS.

section called Detector Module, the detectors SDD1 and SDD2 are enclosed in that module. The ‘Electronics Module’ contains all the other required electronics, like low-noise charge sensitive pre-amplifier (CSPA), Front-end and Processing Electronics (FE-PE), power distribution, and power generation electronics. All of these are accommodated in four different PCBs and mounted inside this module.

As depicted in Figure 5, there are two chains for the analogue processing including the analogue-to-digital converter (ADC). Each chain corresponds to one detector. The output of these ADCs is then fed to a Field Programmable Gated Array (FPGA) for further signal processing in the digital domain. Peak amplitude of the digitized pulse signal due to X-ray interaction with the detectors is the information which is extracted within the FPGA after processing the signal. The final processed energy histograms or the spectra are then transmitted to the Baseline Data Handling (BDH) system of the spacecraft for storage and transmission to ground during ground station visibility. The FPGA also handles the telemetry and telecommand interfaces to the spacecraft for real time health parameter as well as to carry out telecommand operations.

Mechanically, the electronics module consists of a base plate, four machined plates which are attached to the base plate on four sides, and a top plate mounted above these side plates (refer Figure 6). The top plate also supports the detector package as it acts as an anchoring of the seven hollow thermal isolators made of GFRP of the detector module. The low noise signals from the detectors, located in the detector module, are routed through these hollow isolators to the electronics module while the power signals are routed through separate cables outside of these isolators. All PCBs inside the electronics module are stacked through studs separated by spacers (marked in Figure 6). A special nut is press fitted into the base plate and then the stud is passed through this nut. Later the stud is tightened from the bottom side to have a tight box. In the base plate, one M3G DC/DC, X-Y filter card, and one RER type resistor are mounted.

The following subsections detail the electronics module further. The four cards mounted inside the electronics module are named as (mounted from top-to-bottom and in order):

1. Charge Sensitive Pre-amplifier
2. Analogue Front-end and Digital Processing Electronics
3. Power Card, distribution of power to different PCBs and detector units.

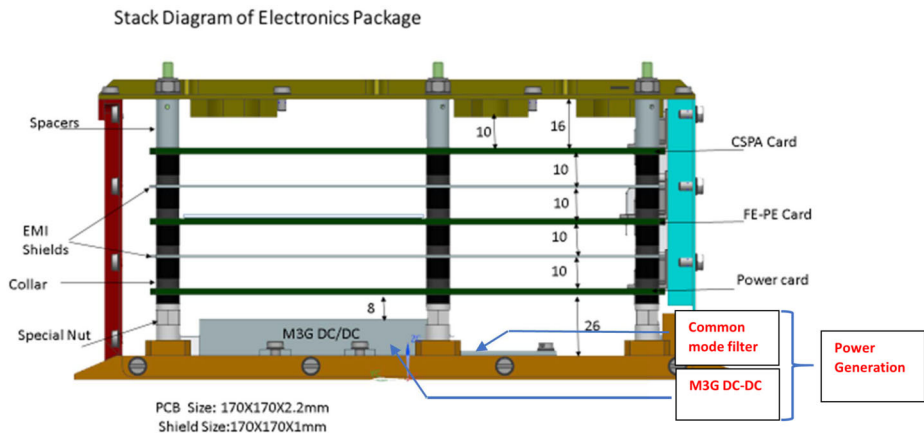


**Figure 6** Electronics Module of SoLEXS. Side covers are not shown to view the inside mounting of the PCBs. The power card marked in this figure is a card which distributes the power to different PCBs and detectors. The power is generated using a combination of a DC-DC converter and a filter card for noise removal as power generation card.

4. Power Generation Card, combination of DC/DC converter along with a filter card marked in Figure 6

#### 4.2.1. Charge Sensitive Pre-Amplifier Board

There are two SDD modules in the detector package. The Analogue Front-end Electronics contains the charge sensitive pre-amplifier (CSPA), low voltage supplies for SDD and CSPA, high voltage bias, and Peltier cooler supply for the SDDs.

The first stage of electronics (internal n-JFET) is integrated into the detector module itself to minimize the noise contribution into the detected charge signal. Also, the detector module contains an inbuilt Peltier cooler, temperature sensor, and an  $8 \mu\text{m}$  thick Be-window to cut-off the optical light. CSPA converts the generated charge signal into equivalent voltage pulses. The CSPA electronics is interfaced to the SDD module with an appropriate interface condition to convert the charge signal into voltage with minimal noise. In SoLEXS, a pulsed reset preamplifier configuration is used for the SDDs to handle high-count rates (of the order of a few tens of thousands) with a charge gain of  $\approx 2 \text{ mV/keV}$  from the first stage low-noise charge sensitive preamplifier. Subsequent to the first stage, there are two more amplification stages to amplify the signals.

High voltages required for the SDD detectors are also generated in this board. The high voltage required to bias the detector module is generated using a PICO DC-DC converter. The output of the PICO converter gives  $-150 \text{ V}$  which is further divided into three different voltages as per detector requirements. Each SDD module draws  $11 \mu\text{A}$  at  $-130 \text{ V}$  current for the internal voltage divider circuit. A common HV circuit is used for both detector modules. The back-contact voltage, the detector bias voltage ( $\text{BC} = -96 \text{ V}$ ), of the module should be within  $\pm 1 \text{ V}$  range, hence to stabilize the PICO input an LM117 regulator is used.

#### 4.2.2. Analogue Front-End and Digital Processing Electronics Board

The output signal from the CSPA PCB is received at the FE-PE PCB. The input waveform from the detected X-ray photon is an exponentially decaying signal which is interfaced to

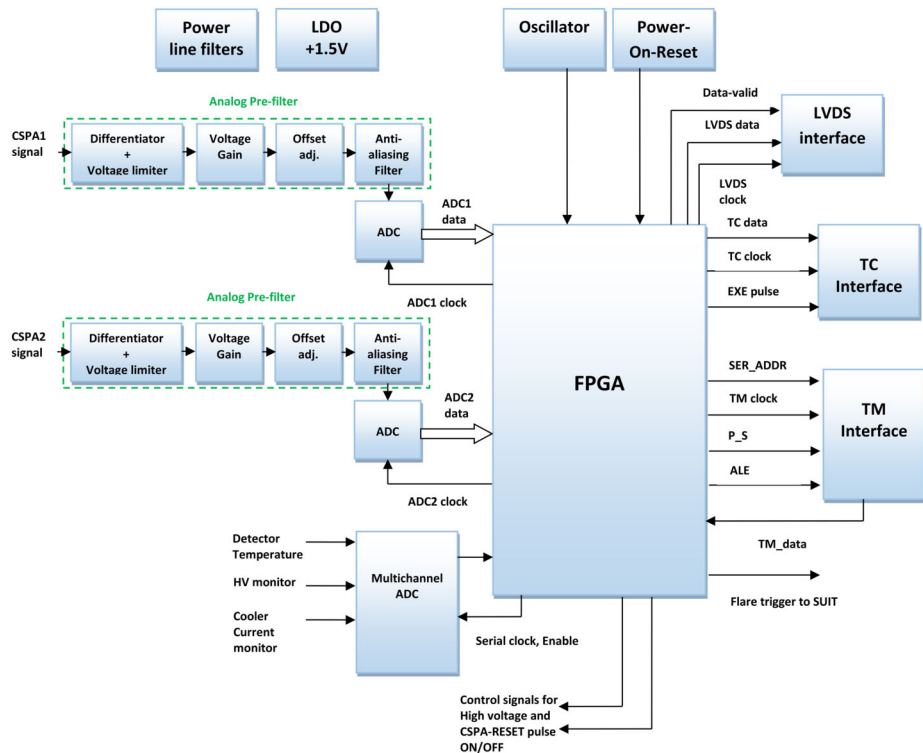


**Figure 7** FE-PE block diagram.

a differential amplifier to provide the required gain, voltage offset and anti-aliasing filtering before sending it to the analogue to digital converter (ADC; RHF1201KSO-01V). It is a 12-bit ADC with 50-mega samples per second (MSPS) capability.

Figure 7 shows the block diagram of the FE-PE card which is mounted below the CSPA card. The analogue pre-filter is the first stage circuit interfacing the CSPA signal from the detector through the CSPA card. The first stage of pre-filter is a  $50\ \Omega$  termination resistor, to limit the incoming signal within the ADC input range, followed by gain stages and an offset adjustment circuit. The anti-aliasing filter rejects the high frequency harmonics before digitization. The ADC for the spectroscopic channel is operated at 20 MHz to capture the rising part of the amplified CSPA analogue signal. Since all the signal processing is carried out in the digital domain, many flexibilities of the processing are enabled. All the digital signal processing is carried out by a Flexible Programmable Gated Array (FPGA) device. Other than the digital pulse processing through FPGA, the FE-PE module also takes care of spacecraft interfaces, like different command sequencing of payload operations, switch on/off of high voltages and SDD reset pulses, HK parameters monitoring etc. For details of the digital pulse processing, the readers are suggested to read Jordanov et al. (1994), Vaghela, Jani, and Mahant (2016).

The health keeping parameters like detector voltage monitor, high voltage monitor, cooler current monitor, etc. are digitized using a multichannel ADC (shown in Figure 7 as multi-channel ADC; ADC128S102QML is used which has a capability of 12-bit digitization with up to 1 MSPS sampling) and the information is stored in the data packet header for later

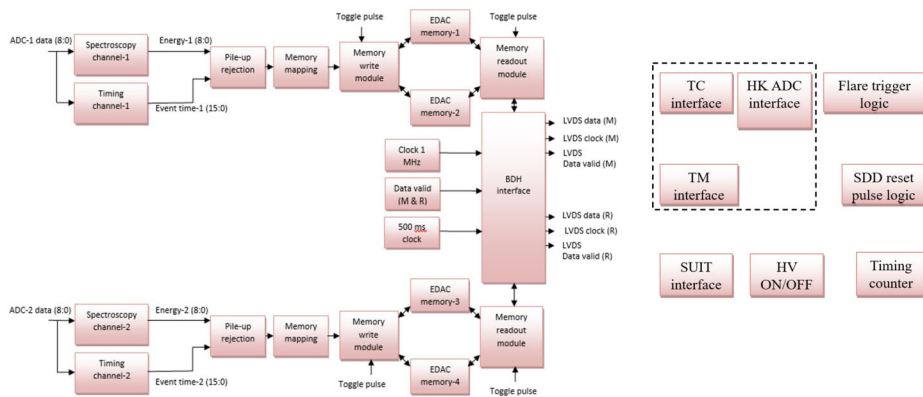


**Figure 8** Block diagram of the FPGA functionalities.

analysis and also sent to telemetry for real time monitoring. The control signals for this ADC are provided by FPGA.

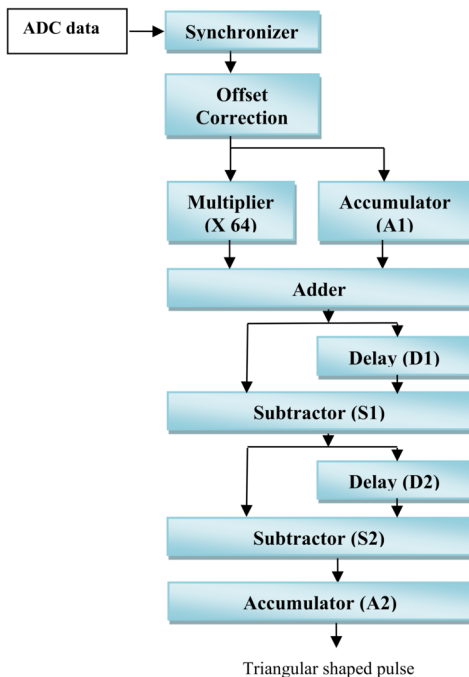
The FPGA carries out all the digital signal processing of SoLEXS payload. Based upon the processing requirements, storage requirements, radiation performance and I/O requirements, the RTAX2000S, from ACTEL, is selected as the signal processing FPGA. The block diagram shown in Figure 8 describes the major signal processing modules internal to the FPGA.

The main and important function of the FPGA is to extract the energy and timing information of the incoming event (or the digitized event from the ADC). This is achieved through a logic. The output of the ADC data is first synchronized to the FPGA clock for proper processing and extracting timing information. Any offset in the pulse is removed through a DC subtraction. Then, the pulse is processed through a combination of multiplier, accumulator, adder, subtractor, and delay logic as shown in the block diagram of Figure 9 to convert the signal into a triangular pulse. The peak of the triangle is then captured as the energy information. The multiplication constant ( $M$ ), as depicted in Figure 9 of the multiplier, is decided by the input RC-time constant and the ADC sample clock ( $M \approx RC\text{-time constant} / \text{sample time period}$ ). The multiplier, accumulator A1, and adder together form a high-pass-deconvolver. The delay ( $D_1$  and  $D_2$ ) as marked in Figure 9 is kept the same to obtain a triangular pulse.

The timing channel also uses the same logic except for a smaller and fixed delay ( $0.5 \mu\text{s}$ ) compared to the spectroscopic channel which uses three variable delays (0.5, 1.0, and  $2.0 \mu\text{s}$ ). These delays in the spectroscopic channel are selectable depending on the count rate and spectroscopic performance requirement. The timing channel will provide the timing information of the event within the  $0.5 \mu\text{s}$  pulse width as soon as the event is captured. This information is used to carry out the pile-up rejection logic on board. Since the pulse is processed in the timing channel, it also gives a coarse spectrum which is stored in three energy bins. The upper energy of the first energy bin and the lower energy of the last energy bin is made programmable by command. This allows us to modify the energy bins in the timing channel anytime during the operation through telecommand.

If multiple events are detected by the timing channel during the processing of a single spectroscopic pulse, the event is considered as piled-up. The indication of multiple pulses will be registered through the timing channel data. The corresponding spectroscopic data will then be rejected. After every single event processing, the peak-hold value is reset in both

**Figure 9** Spectral information generation logic implemented inside the FPGA.



slow and fast channel. Both the spectroscopic and timing pulses are qualified for twelve and three clock cycle durations respectively.

The saturated pulses and wide timing channel pulse rejection logic are also implemented in the FPGA. Hence, there are four conditions to reject a spectroscopic pulse:

- Multiple pulses in the timing channel
- Wide timing pulse
- Pulse saturation
- Low channel counts due to a high rise time

The extracted energy information from the incoming X-ray photon count is stored in histogram format in the on board EDAC memory. The EDAC memory will free-up the FPGA memory slots for further event processing and will also help in protecting the data from radiation events (like single event latch-up). The EDAC module is a 16-bit error detection and correction unit intended for monitoring and correcting data values retrieved from the memory. Extra check bits added at each memory location are programmed by the EDAC during the write cycle. The entire check bits and data combination is verified on read cycles. If any one bit is at fault, then the EDAC will correct the fault and present the corrected 16-bit value to the logic. An error in two bits can be detected but cannot be corrected. The uncorrected error conditions are ignored in our processing.

The FPGA also carries out the following functions:

- Interface to baseband data handling (BDH) for the science data
- Interface to on board computer (OBC) for telemetry and telecommand
- Flare trigger interface to SUIT payload - SoLEXS identifies a sudden increase in count rate continuously for ten seconds and generates a flag which is then sent to the near ultra-

violet imaging payload (SUIT payload) on board Aditya-L1, through a physical interface to the SUIT electronics.

- High voltage and SDD reset sequencing during switch on and off - It is advised by the SDD manufacturer that the pulsed reset to be enabled only when the HV reaches a minimum threshold. To protect the detector, a logic is built in by monitoring the HV input to the detector and pulsed reset is disabled when the HV goes below a set value on board. The set value is configurable through telecommand.
- Data packet formation
- Reference counter to correlate the event trigger time with UT on ground - An accuracy of ten milliseconds is ensured in the UT tagging while processing the SoLEXS data on ground
- Storage of health keeping analogue parameters like detector temperature, high voltage, and cooler current.

#### 4.2.3. Power Generation and Distribution Cards

To meet the power requirements of SoLEXS, an M3G triple output 40 W DC-DC converter is used. The DC-DC converter along with a secondary output filter is housed in the payload base plate package. Various bias required by the payload are generated in the power distribution card, which is mounted below the FE-PE card and above the base plate. Different voltages and power required for SoLEXS were derived using 3T regulators and LDOs.

The spacecraft raw bus is interfaced to the primary side of the M3G DC-DC converter through a relay and a suitably rated fuse. The relay is controlled by a driver circuit which is enabled through external commands from the OBC. This function will allow us to switch on and off SoLEXS manually from the ground command centre. The M3G provides three output voltages, namely + 5 V, + 15 V, and – 15 V. The + 5 V is used for powering all the digital circuits in the payload and also for thermo electric cooler (TEC) of the detector. The ± 15 V are used for powering all the analogue circuits along with the detector high voltage circuit.

The Peltier cooler supply is generated using an LDO and a regulator (LM117). The typical rating for each Peltier is 0.7 W to operate the SDD module at temperature about – 40 °C when the ambient temperature is about – 10 °C.

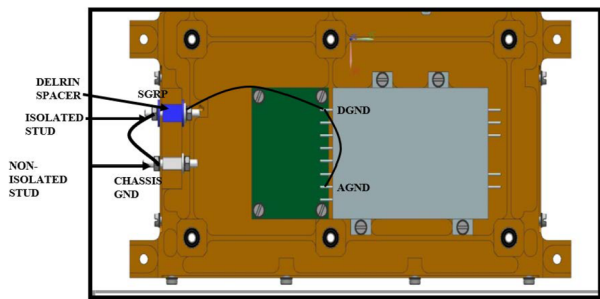
A separate grounding provision is made on the base plate. In this arrangement, two studs are mounted into the base, one stud is directly in contact with base plate and another stud is isolated from the base plate by providing a Delrin bush. The isolated stud serves as electrical isolator from the body of the package.

To eliminate differential and common mode noise, a suitable filter circuit is implemented immediately after the secondary output of the DC-DC converter. Differential filters are connected between line and neutral, to protect against differential mode interference. Common mode filters are designed to filter out the common-mode noise and are connected between the line and chassis. The high power dissipating and box mountable components are placed on the chassis and side wall of the payload.

A type-1 grounding scheme is implemented in SoLEXS in the following way (refer Figure 10):

- Two studs, isolated and non-isolated, are provided on the chassis of the package as shown in Figure 10.
- The isolated stud is the SGRP (Secondary Ground Reference Point). It is electrically isolated from the chassis by means of a Delrin spacer.
- The non-isolated stud is the chassis ground and is shorted to the chassis.

**Figure 10** Grounding scheme used for SoLEXS.



- A wire is brought from the secondary ground of the DC-DC converter and connected to isolated stud inside the package.
- Both studs, which are 20 mm apart, are then connected together from outside the package to connect the SGRP to the chassis with a small 12 AWG wire to make a least resistance path between the SGRP and chassis.

It is to be noted that the Electrical Ground/SGRP is not connected to the package body anywhere inside the SoLEXS package.

## 5. Instrument Characterization

The calibration of an instrument before launch is an essential activity to make sure for a satisfactory performance of the integrated payload to meet the science goals. Calibration activities of SoLEXS include: (i) ground calibration, and (ii) on board calibration. This section briefly discusses the calibration aspects of SoLEXS along with the results obtained. A detailed calibration of SoLEXS is being written up as a separate article which will be published in due course.

### 5.1. Ground Calibration

Ground calibration involves detailed testing and characterization of SoLEXS for the following aspects: (i) spectral calibration for the energy and channel relation to derive the gain and offset, (ii) spectral resolution as a function of energy and temperature, (iii) spectral redistribution function (SRF), (iv) SoLEXS background, and (v) collimator response.

#### 5.1.1. Spectral Calibration: Energy-Channel Relation and Its Temperature Variation

The spectral calibration of SoLEXS is carried out with radioactive sources as well as X-ray fluorescence experiments to derive the energy to channel relation. The left side plot of Figure 11 shows the observed spectral features for the three different experiments. Selected isolated lines were fitted with Gaussians to derive the line center as well as the full-width-at-half-maximum (FWHM).

SoLEXS is configured to have better spectral sampling for energies below  $\approx 8$  keV and double that sampling after that, as all the solar coronal lines are below 8 keV. This configuration minimizes the need for the number of channels and hence the data volume. The right side plot of Figure 11 shows the two linear fitted functions for the derived channel number with that of energy of the spectral feature.

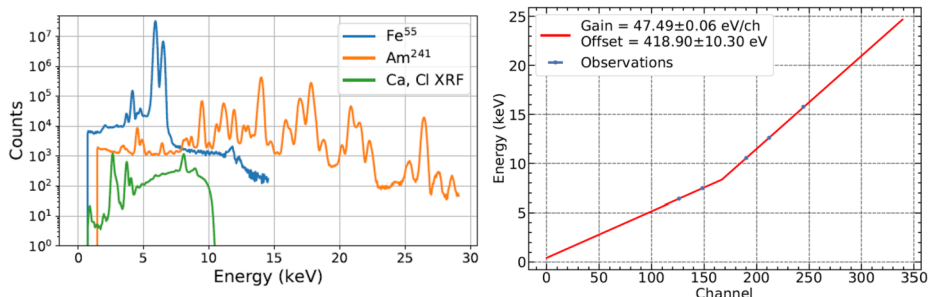


**Figure 11** Left: SoLEXS spectra obtained with two radioactive sources (Fe55 and Am241) along with an XRF experiments of PVC pipe giving characteristic lines corresponding to elements of Ca and Cl. Few isolated lines were selected to estimate the channel number of the line centre. Right: Energy as a function of the derived channel position is shown along with two linear fits (one up to the 167th channel and another from the 168th channel).

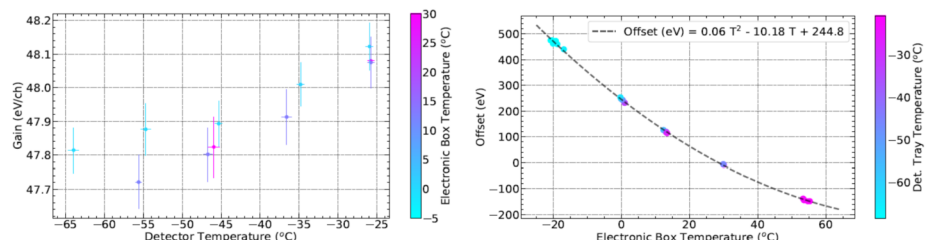


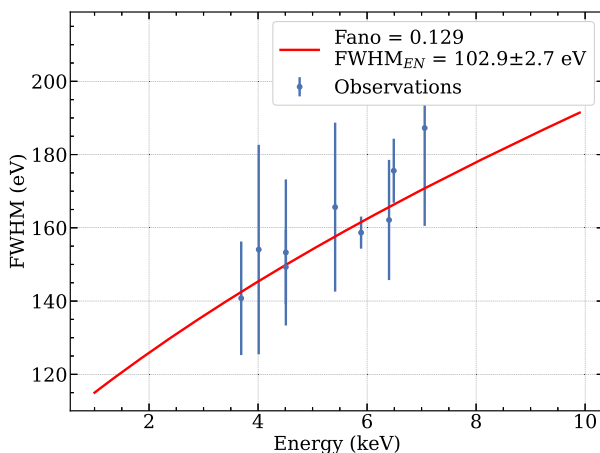
**Figure 12** Gain and offset variation as a function of detector temperature (left) and electronics module temperature (right). The variation of gain with detector temperature is negligible and hence an average value is considered. For the offset, a second order polynomial is fitted and used along with the electronics box temperature measured during on board observations.

The gain and offset variation as a function of temperature (both at the detector and electronics modules) was studied using experiments carried out inside a thermo-vacuum chamber. The detector temperature is one of the measured parameters in the data; it is found to be lower by 30 °C compared to the detector module temperature measured at the detector box. Figure 12 shows the gain (left plot) and offset (right plot) variation as a function of detector and electronics temperature. It is found that the gain does not vary with the electronics box temperature but it has a very small variation with detector temperature (left plot of Figure 12). Hence, the gain value is fixed as an average value for the entire temperature range of SoLEXS operation. The offset is found to be varying with electronics box temperature and not with detector box temperature. This was anticipated as the CSPA is placed inside the electronics module. A second order polynomial is fit for the data obtained from this experiment and used for correcting this offset variation for on board observations.

### 5.1.2. Spectral Calibration: Spectral Resolution with Energy and Temperature

The energy resolution or the FWHM at various incident X-ray energies in the energy range of SoLEXS was also obtained. Figure 13 shows the variation of the FWHM as a function of energy. The model for the FWHM including the fano factor is also shown in this figure. The

**Figure 13** Full width at half maximum (FWHM) for different energy ranges of observations. The model fit is shown as a continuous line while the data points are discrete. The fitted model is used for the Gaussian SRF of SoLEXS. This plot is for the SDD1 detector. For SDD2, the electronics noise  $FWHM_{EN}$  is  $96.9 \pm 8.6$  eV. The fano factor and w are kept the same.



mathematical model used to fit the FWHM as a function of energy is given below:

$$FWHM(E) = \sqrt{FWHM_{EN}^2 + 8 \times \ln(2) \times F \times w \times E}$$

where  $FWHM_{EN}$  is the electronics noise,  $F$  is the fano factor,  $w$  is the mean electron-hole generation energy (3.8 eV for SDD).

The FWHM as a function of temperature was studied using the calibration radioactive source mounted inside the SoLEXS package. This experiment was performed in the thermovacuum chamber. The 24-hour long hot and cold cycle was used for this study using the radioactive source inside SoLEXS. The detector and electronics boxes were kept at different temperature ranges using thermal controls for these tests. The temperatures maintained on the detector and electronics boxes are:

- Detector tray - Cold soak – 40 °C. Hot soak 10 °C
- Electronics box - Cold soak – 20 °C. Hot soak 55 °C
- Detector - Cold soak – 70 °C. Hot soak – 20 °C

The detectors have an inbuilt thermo-electric cooler with a – 30 °C differential temperature with respect to the detector box temperature. It is clear from Figure 14, apart from the initial period, that the FWHM variation is within 10 eV over the full thermal range (from 0 °C to – 40 °C of the detector module).

### 5.1.3. Spectral Redistribution Function (SRF)

The spectral redistribution function (SRF) is a function which defines the mono-energetic response of the system. Any redistribution of flux of mono-energetic X-ray photons to different channels in the system can be obtained from the SRF. To carry out this, an experiment was setup at the Raja Ramanna Centre for Advanced Technology (RRCAT) at Indore using the synchrotron beamline facility. Different mono-energetic input beams were used to obtain the spectra using SoLEXS. Energy peak modelling at different X-ray energies (SRF), including the peak energy, escape peaks from the detector, and the low energy shelves, etc. were carried out and a functional form for the SRF was obtained by defining a hypermet function. Figure 15 shows the functional form of the redistribution function (SRF) obtained through this experiment. It is clearly seen that the redistribution from the prime energy is

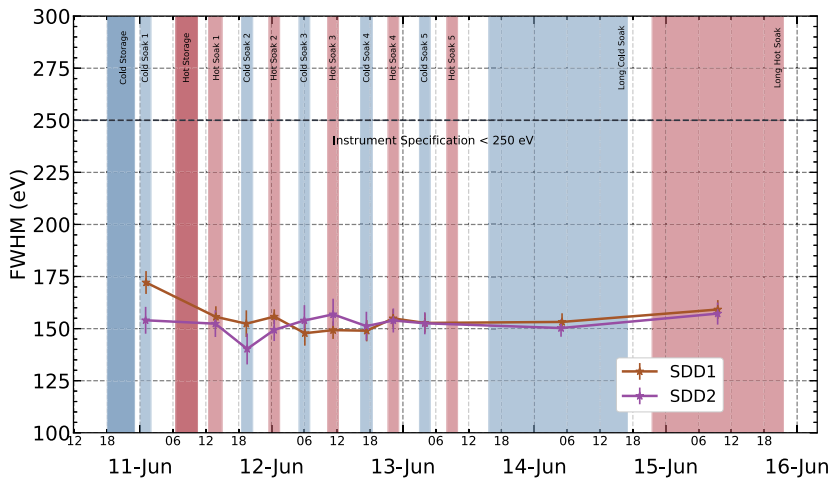


**Figure 14** FWHM as a function of temperature carried out during many days. The hot and cold cycle is marked as a shaded region and the in between periods are for the transition from hot to cold or viceversa. It is clear from this plot that the FWHM does not vary more than 10 eV over the temperature range from 0 °C to –40 °C of the detector module.

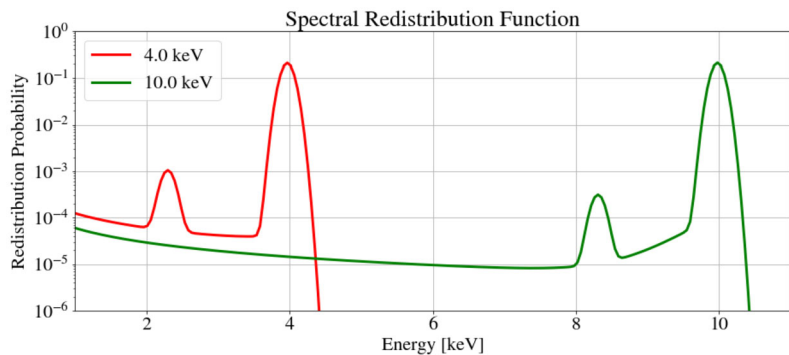


**Figure 15** Spectral redistribution function for different input energies (4 and 10 keV) through the SoLEXS instrument.

three orders lower (the tailing is  $10^{-3}$  times lower than the primary photon). For a typical solar spectrum during a flare, the tailing part would be much less than the photon statistics and it is expected that the off-diagonal element of the SRF may not play a major role in fitting the spectra.

#### 5.1.4. Instrument Background

The instrument background is an important information which needs to be subtracted in order to estimate the true flux of the source. In order to obtain the internal background, SoLEXS was switched on for several days and the data was collected. The background is estimated to be less than  $10^{-3}$  counts sec $^{-1}$ . This background is also observed during the early phase of on board operation with the aperture door closed and also during observations with quiet X-ray sky background at regular intervals.

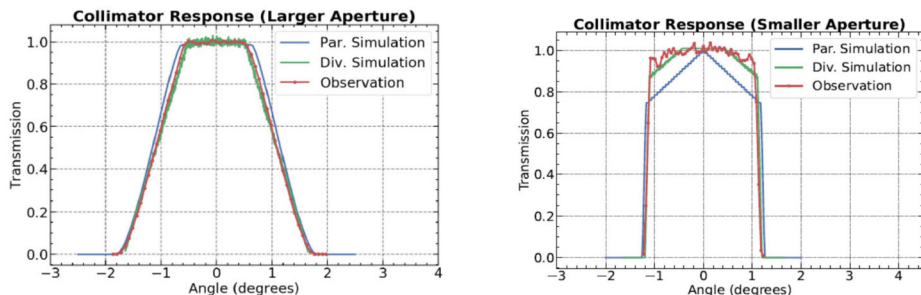


**Figure 16** Collimator response estimated and expected for the larger (left) as well as smaller (right) aperture of SoLEXS. The observation and the divergent input ray (which was used in the experiment) simulation matches quite well. The parallel ray simulation is also shown in this figure to understand the expected collimator response on board.

### 5.1.5. Collimator Response

The response of the collimator to the location of the input source would be required to estimate the flux from the count information of SoLEXS. The effective area calculation would require the collimator response function for different angle of the source with respect to the bore axis of SoLEXS. A laboratory experiment was carried out for different input angles of the source and the differential collimator response was obtained by normalizing to the bore axis of SoLEXS.

Figure 16 shows the collimator response of the larger (left) and the smaller (right) aperture. A source kept at a large distance (about two meters) is used to minimize the effect due to divergence. In order to reproduce the observation, the experimental condition was simulated with the input divergent beam used in the experiment. The experiment and the observations matched quite well giving the confidence to predict the expected collimator response on board for a parallel beam.

## 5.2. On Board Calibration and Performance

In addition to ground calibration, on board calibration of the instrument would help to check for any changes. SoLEXS has an on board calibration source mounted inside the package and this source is seen by the detectors all the time. In addition to this source, it is also planned to observe the Crab nebula which is a standard calibration source in the sky for the energy range of interest for SoLEXS.

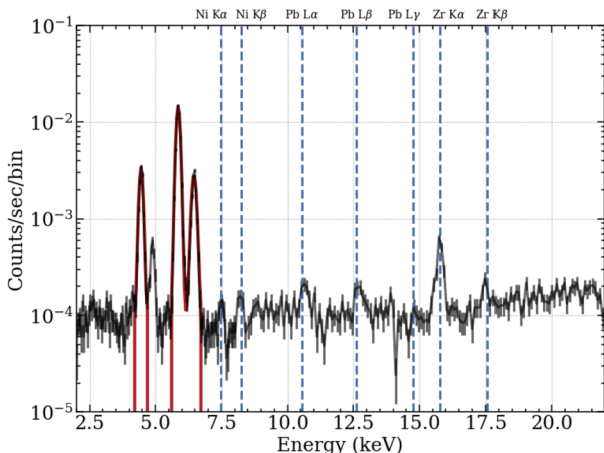
The following aspects are calibrated on board.

- Energy - Channel relation
- FWHM for three different energies corresponding to the calibration source
- Effective area using Crab observations
- Background flux during no source or quiet X-ray sky

### 5.2.1. On Board Internal Calibration Source

In order to carry out calibration on board SoLEXS carries an on board Fe55 source with Ti thin sheet encapsulated in an Al holder providing four spectral lines (K $\alpha$  and K $\beta$  of Mn as well as Ti) at four different energies. This source is mounted inside the SoLEXS detector

**Figure 17** A 48-hour averaged spectra obtained from the SoLEXS instrument (SDD2) on orbit showing the spectral lines of Mn and Ti  $K\alpha$  and  $K\beta$  fitted with Gaussians. There are few other lines seen from the instrument including that of zirconium which was used as collimator inside the SDD module (TOX-SL). This observation is used to verify the energy channel value, the FWHM values, and also the background flux (gain -  $47.52 \pm 0.33$  eV; offset -  $86.66 \pm 39.21$  eV; FWHM at 5.9 keV -  $171.23 \pm 5.9$  eV.



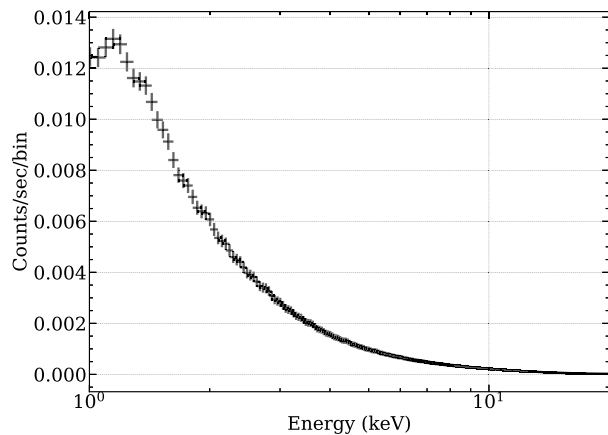
box and hence the detectors are irradiated with this source continuously with a low count rate. A long averaging of the spectra produced during the closed door operation will bring out these spectral lines for calibration purposes.

Figure 17 shows an eighty four hour averaged background spectra obtained in door closed condition on board. The satellite is pointed to the Sun but due to the aperture door mechanism, solar X-ray photons did not reach the detectors and only the on board calibration source along with the high energy cosmic ray particles would be detected by the detector. The on board source which provides photons in Mn and Ti  $K\alpha$  and  $K\beta$  is seen in the lower energy (four emission lines around 5 keV). Three of them (Mn  $K\alpha$ ,  $K\beta$ , and Ti  $K\alpha$ ) are fitted with Gaussians to derive the instrument performance parameters. Figure 17 can be used to verify the on ground calibration parameters for the energy channel, the FWHM for the three energies, and the background of SoLEXS. It is clearly seen that the 170 eV resolution obtained during the thermovacuum testing of the payload is retained ensuring that there were no degradation of the detector during the Earth bound as well as cruise phase of the mission. The entrance aperture door has minimized, if any, the radiation effect on the detector. The gain and offset values were also verified during this test. The background expected from the SoLEXS instrument would be  $10^{-4}$  to  $10^{-3}$  counts per sec per energy bin. Figure 17 also shows the level of other lines due to the SoLEXS instrument and are marked. The zirconium lines are due to the internal zirconium collimators. The lead and nickel lines are due to the soldering used.

### 5.2.2. On Board Crab Observation Plan

In order to carry out the effective area calibration on board, a standard celestial X-ray source, the Crab nebula, will be observed for the X-ray continuum spectra. Crab has a very stable soft X-ray spectrum and hence by comparing the observed spectrum with the expected Crab spectrum along with the detector response, any change in the effective area over time can be estimated and adjusted. A long integration (for about one day) is essential to build the Crab spectrum with good signal-to-noise ratio. Figure 18 shows a typical Crab spectrum simulated for observations for about 6-hours duration with SoLEXS without any background. Observations of Crab for 11-hours are planned which will be carried out when the right opportunity arrives, which includes taking care of all the satellite constraints.

**Figure 18** Crab spectrum for 24-hours duration with SoLEXS (for SDD1). The background is not included in this simulation.



**Table 2** Projected and achieved specifications for SoLEXS.

| Parameter                    | Projected values                           | Observed values  |
|------------------------------|--|--|
| Energy range                 | 1 – 22 keV                                 | 2.0 – 22 keV   |
| Energy resolution            | < 250 eV at 5.9 keV                        | ≈ 170 eV at 5.9 keV  |
| Time cadence                 | Spectral: 1 second<br>Temporal: 0.1 second | Spectral: 1 second<br>Temporal: 1 second                   |
| Detector type                | Silicon Drift Detector (SDD)               | SDD  |
| Active area                  | Two numbers to cover A to X class flares   | Two (SDD1 and SDD2)  |
| Thickness                    | 30 mm <sup>2</sup>                         | 30 mm <sup>2</sup>   |
| Entrance window              | 450  | 450 ± 20 μm  |
| Internal collimator material | 8 μm thick Be                              | 8 μm thick Be  |
| Operating temperature        | Zirconium                                  | – 60 °C – 40 °C  |
| Aperture area                | < – 40 °C                                  | SDD1: 7.069 mm <sup>2</sup><br>SDD2: 0.071 mm <sup>2</sup> |
| Field of view                | SDD1: 7.106 mm <sup>2</sup>                | SDD2: 0.106 mm <sup>2</sup>                                |
| Calibration source           | Sun as a star                              | SDD1: ± 1.8°<br>SDD2: ± 1.3°                               |
|                              | Fe-55 with Ti foil                         | Fe-55 with Ti foil   |

### 5.2.3. Payload Performance on Board

The consolidated on board achieved performance of SoLEXS payload is provided in Table 2. In this table, the projected and achieved specifications are given. Though SoLEXS is able to provide spectra down to 1 keV even in on board observations, the spectral fitting below 2.2 keV needs to be optimized and quantified. Hence, the suggestion is to use spectra from 2.2 keV and above for useful science applications as of now. Similarly, though the temporal cadence of 0.1 second is available in the data, 1 sec temporal data is more reliable and provided to the scientific community.

## 6. Ground System Software and Data Products

Data from SoLEXS payload on board Aditya-L1 spacecraft is received at the Indian Space Science Data Centre (ISSDC) situated at Byalalu, Bangalore. The raw data obtained is then subjected to preliminary processing at ISSDC where the payload data will be packed along with additional information, like housekeeping parameter and SPICE information and this data is defined as Level 0 data. Level 0 data is then sent to the Payload Operations Centre (POC) of SoLEXS situated at the Space Astronomy Group (SAG) of URSC/ISRO. At the POC, the Level 0 data is processed to produce higher levels (L1 and L2) of data products. The data products generated at the POC is then sent back to ISSDC for archival and dissemination to interested users by means of a web site hosted at ISSDC.

In order to process the payload data at the POC, data processing software is developed at the POC. In the following sections, different data products of SoLEXS and the processing methods will be briefly described.

### 6.1. Data Products

Data products of SoLEXS are defined as follows: Level 0 (L0) data is the raw binary data from the payload which is segmented, time tagged, and formatted. The orbit and attitude information of the spacecraft was also provided as SPICE kernels. The time correlation data to UT time is carried out during the L0 processing and provided to the POC. All the house-keeping parameters related to SoLEXS payload, including the temperature of the detector and electronics module are also packaged in the L0.

The L0 data received at the POC is then converted to Level 1 (L1) product after carrying out all instrument related calibrations. The L1 data will contain, good time interval (GTI) information (which time range to be used for science analysis), calibrated one second spectra, and timing data. One full day of observation (0 UT to 23:59:59 UT) will be contained in one L1 file.

Level 2 (L2) data is processed from the L1 spectra. The single temperature model is fitted to the spectral data to derive temperature, emission measure, and abundances and provided as a day-wise file in FITS format. The cadence of this information is dynamically varied depending on the SNR of the spectra. As the model fitting requires good SNR, cadence would be high for flare duration and low during quiet Sun periods.

Along with the L1 and L2 files, calibration data base containing response files as well as background files would be also made available for users to use the L1 data for any other analysis. A flare catalogue is also generated each day along with a light curve image of the day as public outreach product.

### 6.2. Levels of Data Processing

SoLEXS data processing software consists of the following levels of processing

#### 6.2.1. Level 0 to Level 1 Processing

Following are the steps carried out in this level of processing

- Segregation of Level 0 data into SPICE parameters, HK parameters, time correlation table, raw spectrum, and raw light curve files as intermediate files (available only at POC).
- Generation of GTI files based on SPICE and HK parameters for both detectors.
- Generation of one second calibrated spectrum and light curve using raw spectrum file, time correlation table and CALDB for both detectors.
- Generation of flare list and outreach products.

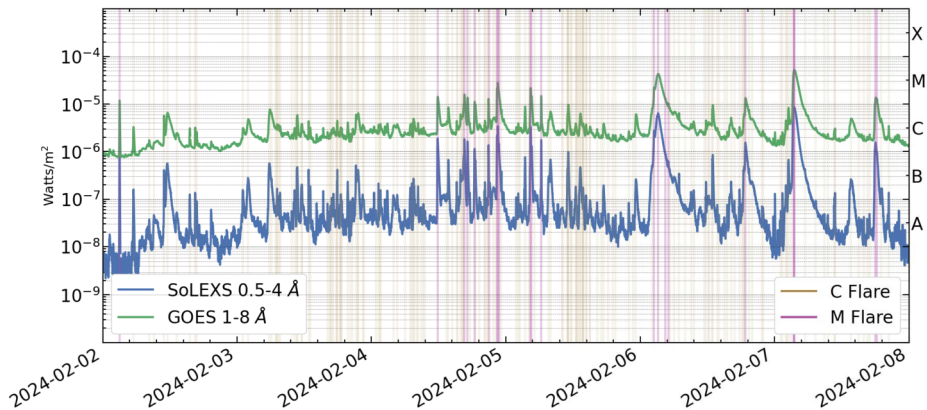


**Figure 19** Light curve of SoLEXS and GOES during the period from February 02 to February 08, 2024. C-class and M-class flares detected by the flare detection algorithm are also marked in this figure.

### 6.2.2. Level 1 to Level 2 Processing

For L1 to L2 data products, spectral fitting using single temperature is carried out to estimate the temperature, emission measure, and abundance. These three parameters will be available as an output data product. CHIANTI databases used along with XSPEC table model to fit the spectra and derive the above three parameters.

The processed L1 data from SoLEXS, is currently available through ISRO science data dissemination system PRADAN (<https://pradan.issdc.gov.in/>). L2 data will be made available soon.

## 7. First-Light Observations

SoLEXS was powered on during October 2023 en route to the Sun-Earth L1 point. During the initial phase, closed aperture door observations were carried out in order to obtain sufficient data for estimating the instrument performance and also obtain the on board instrument background. Figure 17 shows the closed aperture door observations for about eighty four hours. This observation confirmed that the instrument performance is close to the on ground performance. The data also provide a good indication of the instrument background which is of the order of  $10^{-3}$  to  $10^{-4}$  counts per sec per energy bin.

The one-time aperture door mechanism was operated on December 13, 2023. SoLEXS started to receive the X-ray photons from the Sun. From that day onward and until now, SoLEXS has provided continuous coverage of the solar corona in the soft X-ray band. There were one X-class and several M-class flares on the next day of door opening, i.e. December 14, 2023.

Figure 19 shows the light curve of SoLEXS along with GOES from February 02 to 08, 2024. They do not match one to one due to the energy difference of the light curve which is intentionally made to differentiate them in the plot. Several M- and C-class flares were detected by SoLEXS, also marked in this figure.

An M-class flare was also analyzed by fitting the spectrum to derive the coronal physical parameters. Figure 20 shows the observed and isothermal components fitted spectra. Figure 21 shows the temperature evolution (solid thick line with error bars) of the thermal model during the M-class flare observed on February 12, 2024.

**Figure 20** SoLEXS spectra observed during an M-class flare, SOL-2024-02-12T03:46:45, with a integration time of 30 seconds. A single temperature model was fitted to the data and the fitted spectrum is also overplotted.

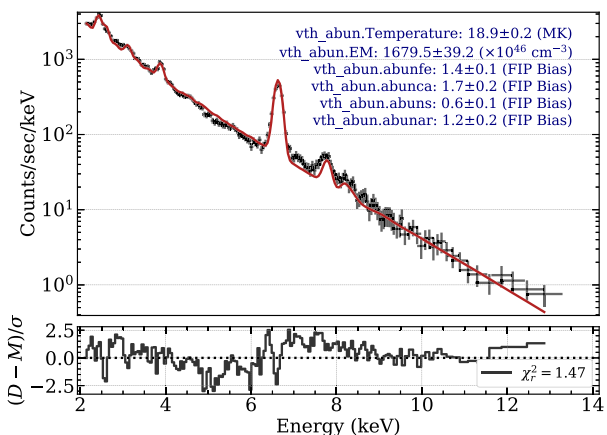
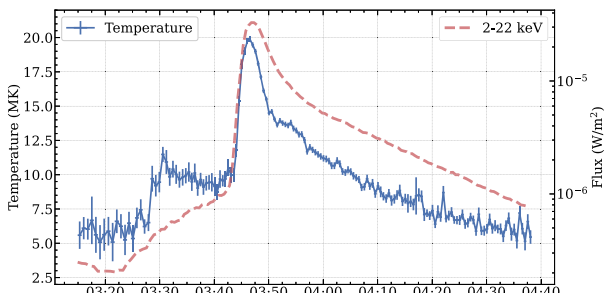


**Figure 21** Temperature estimated by fitting an isothermal model to SoLEXS spectrum observed for an M-class flare on the February 12, 2024, along with the spectral light curves for the energy range of 2 keV to 22 keV.



## 8. Summary

The Solar Low-energy X-ray Spectrometer (SoLEXS) is one of the seven payloads on board Aditya-L1. From Dec 2023 onward, SoLEXS has been observing several hundreds of solar flares every month. From January 06, 2024, day of Sun-Earth L1 insertion, SoLEXS has been operating from L1. From March 2024 onward, SoLEXS operates without any configuration changes on board, providing stable soft X-ray spectra.

The instrument is performing as expected and provides data from 1 keV to 22 keV with a 1 sec cadence. The spectral fitting is also carried out, it is ensured that the fits are good from 2.2 keV and above. Optimization of the fitting below 2.2 keV is under progress and details will be updated as soon as it is ready. SoLEXS L1 data products are made available through ISRO science data dissemination system PRADAN (<https://pradan.issdc.gov.in/>), along with the required user manuals and calibration files. L2 data products will be made available soon. Efforts are on to combine SoLEXS data with the high-energy X-ray spectrometer (HEL1OS) on board Aditya-L1. This would extend the energy range all the way up to 200 keV for big flares. With a 100% duty cycle for X-ray solar observations, SoLEXS will provide unique a data set which is not available from any other mission or observatory and will serve the solar community for the next several years.

**Acknowledgments** SoLEXS is designed and developed at the Space Astronomy Group of U R Rao Satellite Centre (URSC), Indian Space Research Organization, with the help from various entities within URSC. The Thermal System Group provided the required thermal design, analysis, and implementation support. The Mechanism Group developed the required one-time operation mechanism and integrated it into the SoLEXS

payload. The System Integration Group helped in the structural analysis of the payload and participated in the vibration and shock tests. The Reliability and Quality Assurance Group ensured that all non-space grade components are qualified or up-screened for its reliability and quality. The Assembly and Integration Team took the responsibility of integrating the payload to the satellite. The Mission and FDG Team helped in the L0 data generation including the required HK and SPICE data of Aditya-L1. The Indian Space Science Data Centre (ISSDC) and ISRO Satellite Tracking Centre (ISTRAC) are the nodal point of data downloading from the spacecraft and communication with the Payload Operation Centre (POC) and they will be the dissemination centre for the science ready data. The Aditya-L1 project team co-ordinated the overall activities as a nodal point. The POC of SoLEXS is at the Space Astronomy Group of URSC where the higher level data product is generated and posted to ISSDC for dissemination to the scientific community.

Aditya-L1 is an observatory class mission which is fully funded and operated by the Indian Space Research Organization. The mission was conceived and developed with the help from all ISRO Centres and payloads were done by the payload PI Institutes in close collaboration with ISRO and many other national institutes - Indian Institute of Astrophysics (IIA), Inter University Centre of Astronomy and Astrophysics (IUCAA), Laboratory for Electro-optics System (LEOS) of ISRO, Physical Research Laboratory (PRL), U R Rao Satellite Centre of ISRO, Vikram Sarabhai Space Centre (VSSC) of ISRO.

We thank the anonymous referee for providing valuable suggestions to improve the manuscript.

SoLEXS data is available through ISRO science data dissemination system PRADAN (<https://pradan.issdc.gov.in/>)

**Author Contributions** K. Sankarasubramanian is the Principle Investigator for the SoLEXS payload and wrote this paper. Monoj Bug is the primary electronics and instrumentation engineer for the design, development, and testing of SoLEXS. Abhilash Sarwade is involved in the testing, characterization and analysis aspect of SoLEXS. Vaishali Saran is the software developer for SoLEXS. Kumar is the main mechanical engineer for the SoLEXS. Ankur Kushwaha developed the laboratory setup for the collimator response and was also involved in the specification of the mechanism element used in SoLEXS. Smrati Verma is involved in the qualification aspect of SoLEXS mainly the detector socket qualification. M C Ramadevi is involved in the calibration aspects and instrumental in calibration at RRCAT facility for SoLEXS. Lakshmi pathaiah Kiran supported the data analysis and also the calibration at RRCAT for SoLEXS. Mukun Kumar Thakur did the mechanical analysis of the package and also helped in the design of the detector housing of SoLEXS. Kinshuk Gupta and Shalini Maiyya are involved in the detector qualification aspects for TID as well as proton testing for SoLEXS. Also other non-space grade components used in SoLEXS were up-screened and qualified by the team. Nidhi Sharma, Arjun Dey, Srikanth T, and Abhijith Adoni are involved in the thermal design and analysis aspects of SoLEXS. Also involved in the thermal testing aspects, Evangelin Leela Justin and Sajjade Faisal Mustafa are behind the qualification aspects of the SoLEXS. S. Narendra and Shamrao are involved in the mechanism design, development, and implementation aspect of SoLEXS. Motamarri Srikanth, Rethika, Gayathri Malhotra, and Vivek Subramanian are behind the mission, OBC as well as BDH aspects of SoLEXS. Ravi A., Shree Niwas Sahu, Bijaya Kumar Patra, Medasani Thejasree, Narayana Rao, and Murugiah are behind the mechanical integration aspects on the spacecraft for SoLEXS. Vishnu Kishore Pai helped with the EMI/EMC test of SoLEXS. Nashiket Parate helped as a overall project related activities relevant to SoLEXS. Priyanka Upadhyay and Amit Purohit are behind the ground segment raw data and L0 level product generation for SoLEXS. V. Satyanarayana and Kumar Shivam are involved in the ground testing aspects of SoLEXS. Lakshmi A. along with the SoLEXS team carried out the FPGA test case scenarios and also the software aspects

**Data Availability** No datasets were generated or analyzed during the current study.

## Declarations

**Competing Interests** The authors declare no competing interests.

## References

- Alha, L., Huovelin, J., Hackman, T., Andersson, H., Howe, C.J., Esko, E., Väänänen, M.: 2008, The in-flight performance of the X-ray Solar Monitor (XSM) on-board SMART-1. *Nucl. Instrum. Methods Phys. Res., Sect. A* **596**, 317. DOI. [ADS](#).
- Aschwanden, M.J.: 2004, *Physics of the Solar Corona. An Introduction*, Praxis Publishing Ltd., Chichester. [ADS](#).

- Aschwanden, M.J.: 2025, Universal constants in self-organized criticality systems. *Astrophys. J.* **980**, 209. [DOI](#). [ADS](#).
- Aschwanden, M.J., Carolus, Schrijver, J.: 2025, Self-Organized Criticality Across Thirteen Orders of Magnitude in the Solar-Stellar Connection. arXiv e-prints. [arXiv](#). [ADS](#).
- Christe, S., Hannah, I.G., Krucker, S., McTiernan, J., Lin, R.P.: 2008, RHESSI microflare statistics. I. Flare-finding and frequency distributions. *Astrophys. J.* **677**, 1385. [DOI](#). [ADS](#).
- da Silva, D.F., Hui, L., Simões, P.J.A., Valio, A., Costa, J.E.R., Hudson, H.S., Fletcher, L., Hayes, L.A., Hannah, I.G.: 2023, Statistical analysis of the onset temperature of solar flares in 2010–2011. *Mon. Not. R. Astron. Soc.* **525**, 4143. [DOI](#). [ADS](#).
- Del Zanna, G., Mason, H.E.: 2018, Solar UV and X-ray spectral diagnostics. *Living Rev. Sol. Phys.* **15**, 5. [DOI](#). [ADS](#).
- Dere, K.P., Landi, E., Mason, H.E., Monsignori Fossi, B.C., Young, P.R.: 1997, CHIANTI - an atomic database for emission lines. *Astron. Astrophys. Suppl. Ser.* **125**, 149. [DOI](#). [ADS](#).
- Edlén, B.: 1943, Die Deutung der Emissionslinien im Spektrum der Sonnenkorona. Mit 6 Abbildungen. *Z. Astrophys.* **22**, 30. [ADS](#).
- Gilbert, H.R., Alexander, D., Liu, R.: 2007, Filament kinking and its implications for eruption and reformation. *Sol. Phys.* **245**, 287. [DOI](#). [ADS](#).
- Golub, L., DeLuca, E., Austin, G., Bookbinder, J., Caldwell, D., Cheimets, P., Cirtain, J., Cosmo, M., Reid, P., Sette, A., Weber, M., Sakao, T., Kano, R., Shibasaki, K., Hara, H., Tsuneta, S., Kumagai, K., Tamura, T., Shimjo, M., McCracken, J., Carpenter, J., Haight, H., Siler, R., Wright, E., Tucker, J., Rutledge, H., Barbera, M., Peres, G., Varisco, S.: 2007, The X-ray Telescope (XRT) for the Hinode mission. *Sol. Phys.* **243**, 63. [DOI](#). [ADS](#).
- Gopalswamy, N., Shimjo, M., Lu, W., Yashiro, S., Shibasaki, K., Howard, R.A.: 2003, Prominence eruptions and coronal mass ejection: a statistical study using microwave observations. *Astrophys. J.* **586**, 562. [DOI](#). [ADS](#).
- Hannah, I.G., Christe, S., Krucker, S., Hurford, G.J., Hudson, H.S., Lin, R.P.: 2008, RHESSI microflare statistics. II. X-ray imaging, spectroscopy, and energy distributions. *Astrophys. J.* **677**, 704. [DOI](#). [ADS](#).
- Hannah, I.G., Hudson, H.S., Battaglia, M., Christe, S., Kašparová, J., Krucker, S., Kundu, M.R., Veronig, A.: 2011, Microflares and the statistics of X-ray flares. *Space Sci. Rev.* **159**, 263. [DOI](#). [ADS](#).
- Hudson, H.S.: 1991, Solar flares, microflares, nanoflares, and coronal heating. *Sol. Phys.* **133**, 357. [DOI](#). [ADS](#).
- Hudson, H.: 2025, Anticipating solar flares. *Sol. Phys.* **300**, 2. [DOI](#). [ADS](#).
- Huovelin, J., Alha, L., Andersson, H., Andersson, T., Browning, R., Drummond, D., Foing, B., Grande, M., Härmäläinen, K., Laukkonen, J., Lämsä, V., Muinonen, K., Murray, M., Nenonen, S., Salminen, A., Sipilä, H., Taylor, I., Vilhu, O., Walther, N., Lopez-Jorkama, M.: 2002, The SMART-1 X-ray Solar Monitor (XSM): calibrations for D-CIXS and independent coronal science. *Planet. Space Sci.* **50**, 1345. [DOI](#). [ADS](#).
- Jordanov, V.T., Knoll, G.F., Huber, A.C., Pantazis, J.A.: 1994, Digital techniques for real-time pulse shaping in radiation measurements. *Nucl. Instrum. Methods Phys. Res., Sect. A* **353**, 261. [DOI](#). [ADS](#).
- Koleva, K., Dechev, M., Duchlev, P.: 2021, Relations among eruptive prominence properties, flare evolution and CME kinematics in large solar energetic particle events. *J. Atmos. Sol.-Terr. Phys.* **212**, 105464. [DOI](#). [ADS](#).
- Laming, J.M.: 2015, The FIP and inverse FIP effects in solar and stellar coronae. *Living Rev. Sol. Phys.* **12**, 2. [DOI](#). [ADS](#).
- Laming, J.M.: 2021, The FIP and inverse-FIP effects in solar flares. *Astrophys. J.* **909**, 17. [DOI](#). [ADS](#).
- Lee, K.-S., Chae, J., Kwak, H., Cho, K., Lee, K., Kang, J., Lim, E.-K., Song, D.: 2025, Coronal Abundance Fractionation Linked to Chromospheric Transverse MHD Waves in a Solar Active Region Observed with FISS/GST and EIS/Hinode. arXiv e-prints. [arXiv](#). [ADS](#).
- Li, L., Song, H., Hou, Y., Zhou, G., Tan, B., Ji, K., Xiang, Y., Hou, Z., Guo, Y., Qiu, Y., Su, Y., Ji, H., Zhang, Q., Ou, Y.: 2025, Failure of a solar filament eruption caused by magnetic reconnection with overlying coronal loops. *Astrophys. J.* **979**, 113. [DOI](#). [ADS](#).
- Lin, R.P., Dennis, B.R., Hurford, G.J., Smith, D.M., Zehnder, A., Harvey, P.R., Curtis, D.W., Pankow, D., Turin, P., Bester, M., Csillagh, A., Lewis, M., Madden, N., van Beek, H.F., Appleby, M., Raudorf, T., McTiernan, J., Ramaty, R., Schmahl, E., Schwartz, R., Krucker, S., Abiad, R., Quinn, T., Berg, P., Hashii, M., Sterling, R., Jackson, R., Pratt, R., Campbell, R.D., Malone, D., Landis, D., Barrington-Leigh, C.P., Slassi-Sennou, S., Cork, C., Clark, D., Amato, D., Orwig, L., Boyle, R., Banks, I.S., Shirey, K., Tolbert, A.K., Zarro, D., Snow, F., Thomsen, K., Henneck, R., Mchedlishvili, A., Ming, P., Fivian, M., Jordan, J., Wanner, R., Crubb, J., Preble, J., Matranga, M., Benz, A., Hudson, H., Canfield, R.C., Holman, G.D., Crammell, C., Kosugi, T., Emslie, A.G., Vilmer, N., Brown, J.C., Johns-Krull, C., Aschwanden, M., Metcalf, T., Conway, A.: 2002, The Reuven Ramaty High-Energy Solar Spectroscopic Imager (RHESSI). *Sol. Phys.* **210**, 3. [DOI](#). [ADS](#).

- Mawad, R., Abdel-Sattar, W., Farid, H.M.: 2021, An association of CMEs with solar flares detected by Fermi  $\gamma$ -ray burst monitor during solar cycle 24. *New Astron.* **82**, 101450. [DOI](#). [ADS](#).
- Mondal, B., Sarkar, A., Vadawale, S.V., Mithun, N.P.S., Janardhan, P., Del Zanna, G., Mason, H.E., Mitra-Kraev, U., Narendranath, S.: 2021, Evolution of elemental abundances during B-class solar flares: soft X-ray spectral measurements with Chandrayaan-2 XSM. *Astrophys. J.* **920**, 4. [DOI](#). [ADS](#).
- Mondal, B., Vadawale, S.V., Del Zanna, G., Mithun, N.P.S., Sarkar, A., Mason, H.E., Janardhan, P., Bhardwaj, A.: 2023, Evolution of elemental abundances in hot active region cores from Chandrayaan-2 XSM observations. *Astrophys. J.* **955**, 146. [DOI](#). [ADS](#).
- Moore, C.S., Caspi, A., Woods, T.N., Chamberlin, P.C., Dennis, B.R., Jones, A.R., Mason, J.P., Schwartz, R.A., Tolbert, A.K.: 2018, The instruments and capabilities of the Miniature X-ray Solar Spectrometer (MinXSS) CubeSats. *Sol. Phys.* **293**, 21. [DOI](#). [ADS](#).
- Nama, L., Mondal, B., Narendranath, S., Kt, P.: 2022, Abundances of low FIP elements during A-class flares: soft X-ray spectroscopy with Chandrayaan-2 XSM. In: *44th COSPAR Scientific Assembly. Held 16–24 July* **44**, 2571. [ADS](#).
- Narendranath, S., Sreekumar, P., Alha, L., Sankarasubramanian, K., Huovelin, J., Athiray, P.S.: 2014, Elemental abundances in the solar corona as measured by the X-ray Solar Monitor onboard Chandrayaan-1. *Sol. Phys.* **289**, 1585. [DOI](#). [ADS](#).
- Narendranath, S., Sreekumar, P., Pillai, N.S., Panini, S., Sankarasubramanian, K., Huovelin, J.: 2020, Coronal elemental abundance: new results from soft X-ray spectroscopy of the Sun. *Sol. Phys.* **295**, 175. [DOI](#). [ADS](#).
- Ng, M.-H., Zhang, X., Chen, P.F.: 2025, A peculiar feature of the first ionization potential effect before a solar flare impulsive phase observed by MSS-1B, CHASE, and SDO. *Astrophys. J.* **979**, 86. [DOI](#). [ADS](#).
- Raghavendra Prasad, B., Banerjee, D., Singh, J., Nagabushana, S., Kumar, A., Kamath, P.U., Kathiravan, S., Venkata, S., Rajkumar, N., Natarajan, V., Juneja, M., Somu, P., Pant, V., Shaji, N., Sankarasubramanian, K., Patra, A., Venkateswaran, R., Adoni, A.A., Narendra, S., Haridas, T.R., Mathew, S.K., Mohan Krishna, R., Amareswari, K., Jaiswal, B.: 2017, Visible emission line coronagraph on Aditya-L1. *Curr. Sci.* **113**, 613. [DOI](#). [ADS](#).
- Reva, A., Loboda, I., Bogachev, S., Kirichenko, A.: 2024, CME-flare association and the role of reconnection in CME acceleration. *Sol. Phys.* **299**, 55. [DOI](#). [ADS](#).
- Sakurai, T.: 2017, Heating mechanisms of the solar corona. *Proc. Jpn. Acad. Ser. B* **93**, 87. [DOI](#). [ADS](#).
- Sankarasubramanian, K., Sudhakar, M., Nandi, A., Ramadevi, M.C., Adoni, A.A., Kushwaha, A., Agarwal, A., Dey, A., Joshi, B., Singh, B., Girish, V., Tomar, I., Majhi, K.K., Olekar, M., Bug, M., Pala, M., Thakur, M.K., Badagandi, R.R., Ravishankar, B.T., Garg, S., Sitaramamurthy, N., Sridhara, N., Umaphathy, C.N., Gupta, V.K., Agrawal, V.K., Youngdar, B.: 2017, X-ray spectrometers on-board Aditya-L1 for solar flare studies. *Curr. Sci.* **113**, 625. [DOI](#). [ADS](#).
- Schmieder, B., Aulanier, G., Vršnak, B.: 2015, Flare-CME models: an observational perspective (invited review). *Sol. Phys.* **290**, 3457. [DOI](#). [ADS](#).
- Smith, D.M., Lin, R.P., Turin, P., Curtis, D.W., Primsch, J.H., Campbell, R.D., Abiad, R., Schroeder, P., Cork, C.P., Hull, E.L., Landis, D.A., Madden, N.W., Malone, D., Pehl, R.H., Raudorf, T., Sangsingkeow, P., Boyle, R., Banks, I.S., Shirey, K., Schwartz, R.: 2002, The RHESSI spectrometer. *Sol. Phys.* **210**, 33. [DOI](#). [ADS](#).
- Sylwester, J., Gaicki, I., Kordylewski, Z., Nowak, M., Kowalski, S., Sjarkowski, M., Bentley, W., Trzebinski, R.D., Whyndham, M.W., Guttridge, P.R., Culhane, J.L., Lang, J., Phillips, K.J.H., Brown, C.M., Doschek, G.A., Oraevsky, V.N., Boldyrev, S.I., Kopaev, I.M., Stepanov, A.I., Klepikov, V.Y.: 1998, RE-SIK: high sensitivity soft X-ray spectrometer for the study of solar flare plasma. In: Priest, E.R. (ed.) *Crossroads for European Solar and Heliospheric Physics. Recent Achievements and Future Mission Possibilities*, *ESA Special Publication* **417**, 313. [ADS](#).
- Temmer, M.: 2021, Space weather: the solar perspective: an update to Schwenn (2006). *Living Rev. Sol. Phys.* **18**, 4. [DOI](#). [ADS](#).
- Tripathi, D., Ramapakash, A.N., Khan, A., Ghosh, A., Chatterjee, S., Banerjee, D., Chordia, P., Gandorfer, A., Krivova, N., Nandy, D., Rajarshi, C., Solanki, S.K.: 2017, The solar ultraviolet imaging telescope on-board Aditya-L1. *Curr. Sci.* **113**, 616. [DOI](#). [ADS](#).
- Upendran, V., Tripathi, D., Mithun, N.P.S., Vadawale, S., Bhardwaj, A.: 2022, Nanoflare heating of the solar corona observed in X-rays. *Astrophys. J. Lett.* **940**, L38. [DOI](#). [ADS](#).
- Vadawale, S.V., Shanmugam, M., Acharya, Y.B., Patel, A.R., Goyal, S.K., Shah, B., Hait, A.K., Patinge, A., Subrahmanyam, D.: 2014, Solar X-ray Monitor (XSM) on-board Chandrayaan-2 orbiter. *Adv. Space Res.* **54**, 2021. [DOI](#). [ADS](#).
- Vaghela, M., Jani, R., Mahant, K.: 2016, FPGA implementation of digital pulse processing techniques for radiation measurement. In: *2016 International Conference on Microelectronics, Computing and Communications (MicroCom)*, 1. [DOI](#).

- Valluvan, A.B., Goyal, A., Jain, D., Samantaray, A.S., Sarwade, A., Sankarasubramanian, K.: 2024, Solar flare catalogue from 3 years of Chandrayaan-2 XSM observations. *Sol. Phys.* **299**, 8. [DOI](#). [ADS](#).
- Yashiro, S., Gopalswamy, N.: 2009, Statistical relationship between solar flares and coronal mass ejections. In: Gopalswamy, N., Webb, D.F. (eds.) *Universal Heliophysical Processes, IAU Symposium* **257**, 233. [DOI](#). [ADS](#).

**Publisher's Note** Springer Nature remains neutral with regard to jurisdictional claims in published maps and institutional affiliations.

Springer Nature or its licensor (e.g. a society or other partner) holds exclusive rights to this article under a publishing agreement with the author(s) or other rightsholder(s); author self-archiving of the accepted manuscript version of this article is solely governed by the terms of such publishing agreement and applicable law.